Journal of Physics Communications

Neutron Compton Scattering: from proton momentum distribution to muonium hyperfine coupling constant in the isopropyl radical

Matthew Krzystyniak ⬛ , Francis Pratt and Giovanni Romanelli ⬛

ISIS Facility, Rutherford Appleton Laboratory, Chilton, Didcot, OX11 0QX, United Kingdom

E-mail: matthew.krzystyniak@stfc.ac.uk

Abstract

We establish a fast and reliable benchmarking protocol for predictions of Muon Spin Resonance observables. To this end, we apply neutron Compton scattering (NCS) to study the nuclear momentum distributions of the proton and deuteron in the condensed phase of the isopropyl and d-isopropyl alcohols. By subtracting the time-of-flight NCS spectra of both compounds we demonstrate that the proton momentum distribution in the OH group of isopropanol and the deuteron momentum distribution in the OD group in d-isopropyl can be studied selectively. The site-selective application of the NCS method enables the calculation of the magnitude of the frequency isotope effect for the proton in OH along the hydrogen bond direction. By comparing the magnitude of the frequency isotope effect with values predicted for simple model potentials we are able to perform the appraisal of the degree of anharmonicity of the OH proton environment. Assuming that the effective potential felt by the OH proton along the hydrogen-bond direction can be satisfactorily described by the Morse potential, we are able to calculate its dissociation constant D and decay constant a. Finally, assuming that the same Morse potential describes the local binding of Muonium in the mioniated isopropyl radical, we are able to predict its width of momentum and position distributions and the kinetic and zero-point energy. Based on these results, we are able to provide a conservative bound for the magnitude of the isotope effect on the muonium hyperfine interaction without resorting to a complicated and computationally expensive methodology based on the application of path integrals.

1. Introduction

1.1. Muon spin rotation and its challenges

Materials science at the nanoscale over last few decades has profited from (and largely owed its success to) the development of a few very special and unique spectroscopic techniques that do not have the stigma of being volume-averaged. One of the most prominent examples of such a development owing to the site-specific method sensitivity is the muon spin resonance (μSR) [1]. The supremacy of μSR over volume-sensitive nuclear magnetic resonance (NMR) is best manifested in the spin spectroscopy of the solid-state where the interpretation of μSR spectra is greatly simplified by the absence of spectral line broadening due to the lack of the long-range spin-spin couplings (otherwise present in the NMR spectra) thanks to the local detection character of the muon, acting as a local magnetic moment probe [2]. Namely, instead of a static NMR coil wound around a macroscopic volume of a sample, one has a fast-moving 'coil-projectile', the muon particle, picking up signals from local magnetic environments. During the muon's 2.2 μs lifetime, muonium can enter into compounds such as muonium chloride (MuCl) or sodium muonide (NaMu) [3]. Due to the mass difference between the antimuon and the electron, muonium (μ + e−, hereinafter Mu) is more similar to atomic hydrogen (p + e−) than positronium (e + e−) [3]. Its Bohr radius and ionization energy are within 0.5% of hydrogen, deuteron, and tritium, and thus it can usefully be considered as an exotic light isotope of hydrogen with a mass of l/9 of H [3].

The modelling of Mu in condensed matter systems up to date has dealt with properties such as Mu formation in gases, liquids, and solid insulators, and the rate constants of its reactions with molecules [2]. Despite the unquestioned success in the experimental department, also μSR is not entirely free from problems as far as *ab initio* modelling is concerned [3]. The main challenge here is due to the fact that the Zeeman interaction of the unpaired electron, the muon and of additional nuclei, as well as the electron-muon and electron-nuclear hyperfine interaction, lead to very complicated μSR spectra [4]. The variation of the muon-electron coupling constants with radical structures is similar to that of the analogous known proton-electron coupling constants. However, the small muon mass greatly amplifies any vibrational isotopic effect in these coupling constants as well as all other properties dependent on the vibrations of the radical. One could anticipate that for muonium adduct molecules, the isotope effect is so large that the Born–Oppenheimer approximation (BOA) is invalid, a situation certainly rarely encountered in the case of *ab initio* modelling of electronic and nuclear degrees of freedom in condensed-matter systems. For isotopomers of the H_2^+ molecule Webster and McKenna showed by a series of non-adiabatic calculations beyond the Born–Oppenheimer approximation, that the key isotope effect arises through the mass dependence of the zero-point vibrational energy [5]. On the whole, one has to anticipate that the Mu-adduct species sample points on a property surface well distant from the equilibrium position. For example, a variation-perturbation approach, applied to investigate isotope-dependent zero-point vibrational corrections to one-electron properties of a MuMu adduct water molecule in its ground electronic state, has shown that the root-mean-square displacement involving the O–Mu internuclear distance is ca. 11 pm with a root-mean-square displacement in the internuclear angle for MuOH of 12.73 degrees and MuO of 14.71 degrees [5]. *Ab initio* modelling under such circumstances is very difficult, rendering most DFT methods treating nuclei classically within the BOA completely unusable. This can be demonstrated owing to the recent rapid development of Path-Integral Molecular Dynamics (PIMD) modelling methods [6]. For example, the on-the-fly *ab initio* density functional PIMD simulations, which can account for both the nuclear quantum effect and thermal effect, when applied to the evaluation of the structures and isotropic hyperfine coupling constants (HFCCs) for muoniated and hydrogenated acetone radicals *in vacuo*, exposes dramatic deficiencies of the DFT methodology with classical nuclei. The HFCC value from a simple geometry optimization calculation without both the nuclear quantum effect and thermal effect is 8.18 MHz, and that by standard *ab initio* molecular dynamics simulation with only the thermal effect and without the nuclear quantum effect is 0.33 MHz at 300 K, where these two methods cannot distinguish the difference between muoniated and hydrogenated acetone radicals. In contrast, the reduced HFCC value of the muoniated acetone radical by the PIMD simulation is 32.1 MHz, which is about 8 times larger than that for the hydrogenated radical of 3.97 MHz with the same level of calculation [6].

1.2. The need for a mass and site-selective dynamic probe

The calculation of many properties of muoniated radicals starts from the appraisal of the extent of quantum delocalisation of Mu, both in momentum and position representation. In general, the momentum distribution can be obtained from the Fourier transform of the end-to-end-distribution of the linear (or 'open') polymer PIMD calculation, but not from the ring (or 'closed') polymer PIMD. Moreover, the PIMD methods using generalised Langevin equation (PI-GLE) approach employ a 'trick' for avoiding the need for a large number of replicas, as far as the physical temperature of the system is low. However, it is only by using this 'artificial noise' thermostat with adequate and well-tested parameters that one can create random fluctuations in the motion of the nuclei which are similar to the zero-point broadening of the real quantum delocalization. To speed up the calculations and base them on the closed-path PIMD scheme, one might resort to an additional approximation that the nuclear wave function is node-free so that it can be obtained as the square root of the nuclear density in coordinate-space, or the square root of the Fourier transform of nuclear momentum distribution.

However, despite the sophistication of the PIMD-based methodology, the results calculated *in vacuo* will always be far off the real values measured in bulk systems as the explicit presence of solvent molecules has a major effect on *in vacuo ab initio* calculations for the quantitative reproduction of experimental data. Clearly, there is a need for a quick and model-free method for the appraisal of properties of muoniated radicals under realistic bulk conditions. In this context, the employment of the Deep Inelastic (DINS), or neutron Compton Scattering (NCS) seems a plausible choice. NCS, as the only neutron-based spectroscopic technique, offers true mass selectivity by recording a combination of Doppler-broadened recoil peaks for different nuclei present in the sample of interest [7–19]. Moreover, in the limit of the incoherent and impulse approximations, valid in NCS, the width of a Doppler-broadened NCS peak of a given nucleus is proportional to its nuclear momentum distribution, $n(p)$, being the square of the absolute value of the Fourier transform of the spatial wave function [7–19]. Importantly, the small mass of the proton/deuteron (H/D) leads to an NCS recoil peak that is well separated from the peaks of heavier nuclei, which appear as nearly elastic contributions. This feature, in
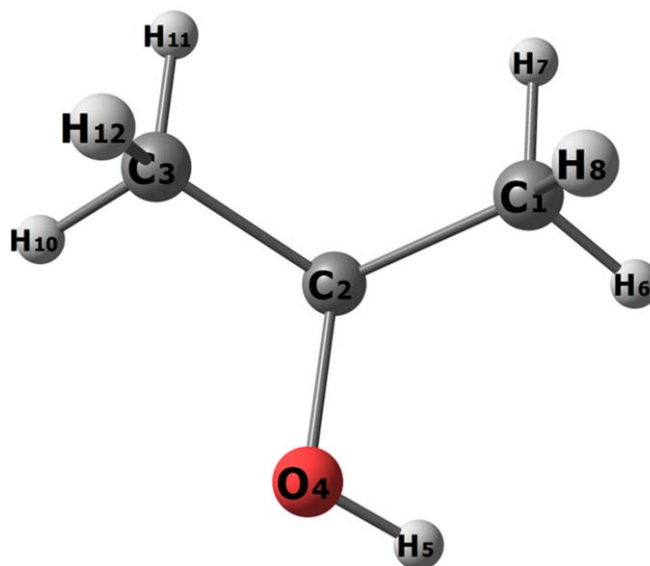
Figure 1. The molecular structure of isopropyl alcohol and d-isopropyl alcohol. The colour indicates the type of atoms: oxygen (red), carbon (dark grey), and hydrogen (light grey). Atom labels correspond to the standard configuration used as input for the *ab initio* calculations. For d-isopropyl alcohol, the hydrogen atom in the OH group (H5) is replaced with a deuteron (D5). The H9 hydrogen atom (not shown), attached to the C2 carbon atom, is perpendicular to the figure plane with the C2–H9 bond facing downwards. See text for details.

combination with the fact that NCS is sensitive to total bound scattering cross-sections, makes muoniated radicals containing H and D ideal candidates for the NCS measurements.

This contribution seeks to pave the way towards establishing a robust model-free protocol for the appraisal of basic properties of the muoniated radicals and a reliable benchmarking protocol for the PIMD-based predictions. As a feasibility study of the newly proposed computational protocol, we analyse here the results of NCS measurements on two model bulk systems with a similar local environment around the OH group, the isopropyl and d-isopropyl alcohol (figure 1).

The idea to perform a tandem NCS measurement of a native and deuterated counterpart of the same molecular system, both differing only in the presence (or absence) of H(D) in the OH group, renders an otherwise mass-selective technique also site-selective. Namely, by virtue of the mass-selectivity, the direct NCS measurement of the deuterated compound yields the characterisation of the deuteron momentum distribution in the OD group. Furthermore, by subtracting the NCS spectra of both compounds one obtains the selective spectrum of the proton momentum distribution in the OH group of the isopropanol molecule that can then be compared with the deuteron momentum distribution in the OD group in d-isopropyl. This site-selective application of the NCS method enables the calculation of the magnitude of the frequency isotope effect for the proton in OH along the hydrogen bond direction. By comparing the magnitude of the frequency isotope effect with values predicted for simple model potentials we are able to perform the appraisal of the degree of anharmonicity of the OH proton environment. Assuming that the effective potential felt by the OH proton along the hydrogen bond direction can be satisfactorily described by the Morse potential, we are able to calculate its dissociation constant D and decay constant a. Finally, assuming that the same Morse potential describes the local binding of Muonium in the mioniated isopropyl radical, we are able to predict its width of momentum and position distributions and the kinetic and zero-point energy. Moreover, based on the latter results we provide a conservative bound for the magnitude of the isotope effect for the hyperfine interaction of the muonium in the muoniated isopropyl in the condensed phase, all without resorting to a complicated and computationally expensive methodology based on the application of path integrals.

2. Materials and methods

We have performed neutron experiments on isopropanol and isopropanol-2-d_1 (hereafter referred to as d-isopropanol), at 250 K and 300 K, by concurrently applying the mass-selective NCS (MANSE), enabling distinct separation of H and/or D peaks, and neutron transmission (NT) at the VESUVIO+ beamline in the Target Station 1 (TS1) of the ISIS pulsed neutron and muon source at the Rutherford Appleton Laboratory, UK [10, 14, 20–29].

Isopropanol (99.0%) and d-isopropanol (98.0%) neat liquid samples were purchased from Sigma-Aldrich. Two square-shape (90 × 90 mm^2) aluminium containers for liquid samples were used for the experiments: one of 0.5 mm thickness for the isopropanol sample, and one of 1.8 mm thickness for the d-isopropanol sample. Both liquids were loaded into the containers through a pair of small inlets in the containers front walls using a set of syringes. Following this, the inlets were sealed. The empty containers were then separately measured at the same temperatures as the samples. Both sample and empty-container neutron transmissions were measured as a function of the incident neutron energies, normalising to the transmission spectrum of the empty instrument, a protocol routinely applied in broadband transmission experiments on VESUVIO [30–34]. The mass of the isopropanol sample was 0.89 g. Given the total bound scattering cross-section values of H, C, and O and the sample stoichiometry, C_3H_8O, the mass of 0.89 g corresponded to the sample transmission for epithermal neutrons (above the incident neutron energy of 1 eV) at the level of 0.86. The mass of the d-isopropanol sample was 1.58 g, which, given the sample stoichiometry, C_3H_7OD, resulted in the sample transmission for epithermal neutrons at the level of 0.82.

The NCS data treatment has been described in great detail elsewhere [9, 10, 35] and thus only the main points will be mentioned here. In essence, in the Impulse Approximation[36] limit, a MANSE spectrum measured by a particular detector (at a given scattering angle θ) and at a given time-of-flight (TOF) value, t, is a sum of neutron Compton recoil peaks. Mathematically, [9, 10]

$$C(\theta, t) = \frac{E_0 I(E_0)}{q} \sum_M c_M J_M(x_M) \otimes R_M(x_M) \qquad (1)$$

where M is the mass of a given nuclear isotope (H, D, C, O from the samples and Al from sample containers), E_0 and $I(E_0)$ are the incident neutron energy and intensity, respectively, and q is the neutron momentum transfer. The Compton profile for a given mass M was fitted with an expression of the form $J_M(x_M) \otimes R_M(x_M)$ with $J_M(x_M)$ given by [9, 35]:

$$J_M(x_M) = \frac{e^{-x_M^2}}{\sqrt{2\pi\sigma_M^2}}\left(1 - \frac{\sigma_M \frac{\sqrt{2}}{12}}{q} H_3(x_M)\right) \qquad (2)$$

where $J_M(x_M)$ is the unit-area-normalised longitudinal momentum distribution (NMD) of a nucleus of mass M, and x_M defined as $x_M = \frac{y_M}{\sigma_M \sqrt{2}}$ with y_M being the longitudinal nuclear momentum for a given nuclide of mass M, and σ_M is the standard deviation of $J_M(x_M)$ measured in the units of Å^{-1}. In fitting the NCS data stoichiometric constraints are applied. The ratios of the relative recoil peak intensities, c_M, are fixed according to the values of the products of the respective total bound scattering cross-sections and numbers of nuclei of a given type per sample formula unit [37–40]. Equation (1) also includes a convolution product ($\otimes$) with a mass-dependent resolution function, $R_M(x_M)$ [9, 35]. The second term in equation (2) accounts for deviations from the impulse approximation, also known as final state effects (FSEs), expressed here in the isotropic lattice limit through the third-order Hermite polynomial, $H_3(x_M)$ [9, 10, 35].

The raw NCS data were reduced using newly developed routines implemented in the MantidPlot computational environment [41, 42]. An iterative procedure was applied for NCS data, recorded in the time-of-flight (TOF) domain by 48 VESUVIO+ forward scattering detectors at 250 K and 300 K for isopropanol, d-isopropanol as well as the empty aluminium containers (hereinafter referred to Al NCS data). The iterative NCS data treatment protocol consisted of the following steps:

1. Raw NCS data were pre-fitted, using equation (1), in order to find the initial intensities and widths of H (D), C and O peaks of the samples as well as Al peaks;

2. the obtained average values of the peak widths and stoichiometrically fixed relative peak intensities were input into the algorithm calculating the sample-dependent gamma and multiple-scattering background;

3. gamma and multiple-scattering background was subtracted from the raw NCS data;

4. a new fit using equation (1) of NCS data after the subtraction of gamma and multiple-scattering background was performed with the aim of obtaining the second approximation to the average values of peak widths;

5. a new set of average peak widths together with fixed relative intensities formed an input to the algorithms simulating the second approximation to the shapes of multiple scattering and gamma background corrections;

6. the final subtraction of gamma and multiple scattering corrections was performed;

7. after the subtraction of the backgrounds, a final fit of peak widths was performed and the final averaged values of the peak widths and relative peak intensities were obtained;

8. fitted curves of the recoil peaks from masses other than the proton and the fitted curves representing the FSE contributions to the proton recoil peaks (see the second term in equation (2)) were subtracted and the corrected TOF NCS data;

9. the isolated TOF NCS proton recoil peaks were focused in the longitudinal momentum space of the proton (hereafter referred to as the proton Y space data) for precision fitting of the proton NMD using purely Gaussian expression (expressed as the first part of equation (2));

10. in the case of the TOF NCS deuteron recoil peaks, no longitudinal momentum space focusing was performed and the final values of the D peak widths were obtained as averages over sequential, detector-by-detector, fitting of the TOF NCS spectra containing D recoil peaks;

11. in order to obtain the proton momentum distribution of the proton in OH, a purely Gaussian fit of the difference between the focussed proton Y space data of isopropanol and d-isopropanol was performed. Before subtraction, the proton Y space data of d-isopropanol were scaled by the factor of 7/8 reflecting the ratio of the number of protons in the formula units of both systems.

Before we proceed to the detailed description of the main steps of NCS data treatment, outlined in points 1–11 above, illustrated in figure 2, one important remark is in order. As described in points 9–11 of the protocol, the recoil peak of hydrogen and deuteron undergo a completely different treatment. The deuteron recoil peaks are fitted sequentially, detector-by-detector, and the values of the fitted widths are recorded in order to be averaged over the entire range of detectors used in the data analysis. The proton recoil peaks, however, after being provisionally fitted on the detector-by-detector basis, undergo further treatment. They are isolated in the TOF domain, transformed into the longitudinal momentum domain and then focused and rebinned in this latter domain for higher precision fitting. Due to this substantial difference in the treatment, the proton and deuteron recoil peak fitting cannot be easily illustrated in on simple graph. Mathematically, the focusing of proton recoil peaks in the proton longitudinal momentum space without their prior isolation (and thus retaining the deuteron recoil peaks in the focused spectra) would always result in smearing out the deuteron recoil peaks, a kinematic effect due to different loci of the proton and deuteron recoil lines for each scattering angle (detector). Converesely, fitting the TOF NSC spectra sequentially, detector-by-detector, does not allow for the longitudinal momentum space focusing of either of the two recoiling nuclear species. Thus, as an illustration, in figure 2 the TOF NCS data treatment scheme is shown only for one chosen VESUVIO detector. Such choice retains the possibility of graphically showing the logic behind the data treatment with one drawback, however. Namely, the procedure of the focusing of the proton NMD in the proton longitudinal momentum space is illustrated only as a mathematical transformation without showing their added benefit of increasing the signal-to-noise ratio of the proton recoil peak data and thus the precision of the proton NMD fit.

Figure 2 shows data recorded for isopropanol and d-isopropanol at the temperature of 300 K. The data were recorded by the detector placed at a distance of 0.52 metres from the sample position in the forward scattering direction at a scattering angle of 63.4 degrees. The position and scattering angle values pertaining to this detector were obtained via a separate calibration procedure described elsewhere [22, 23]. The TOF NCS data, prior to further analysis, were rebinned between 110 and 385 microseconds with a bin width of 3 microseconds. The lower binning boundary was set to a relatively high value of 110 microseconds, a procedure routinely applied in NCS data reduction in order to avoid the contamination of the TOF NCS signals with spurious signals from resonant neutron absorption in the Au foils of the VESUVIO detection setup [25–27]. It is worth noting that this procedure does not affect the precision of the fitting of the width of the proton NMD. The reason for this is twofold. Firstly, the width of a Gaussian profile can be very robustly estimated from the fits of the recoil peaks as most of the peak profile is anyway retained between 110 and 385 microseconds. Secondly, the fit precision is augmented by the presence of an additional physical constraint, the requirement that an NMD be an even function of the longitudinal momentum distribution variable Thus, in principle, it is enough to record one shoulder of an NMD and then apply symmetrization in order to recover the full profile [9–11, 14, 15, 18, 19, 43–45].

The top and middle panels of figure 2 show the raw and the corrected, after the subtraction of the gamma and multiple scattering background, TOF NCS data for d-isopropanol and isopropanol, respectively. It is worth noting that upon subtraction of both types of background the magnitude of the errorbars of the TOF NCS data does not increase. The reason for this is twofold. Firstly, the gamma-background correction is a result of the application of an analytical, and thus smooth, function of the time of flight [46]. Secondly, the multiple scattering correction, being a result of a Monte-Carlo-type calculation, can be made arbitrarily noiseless by
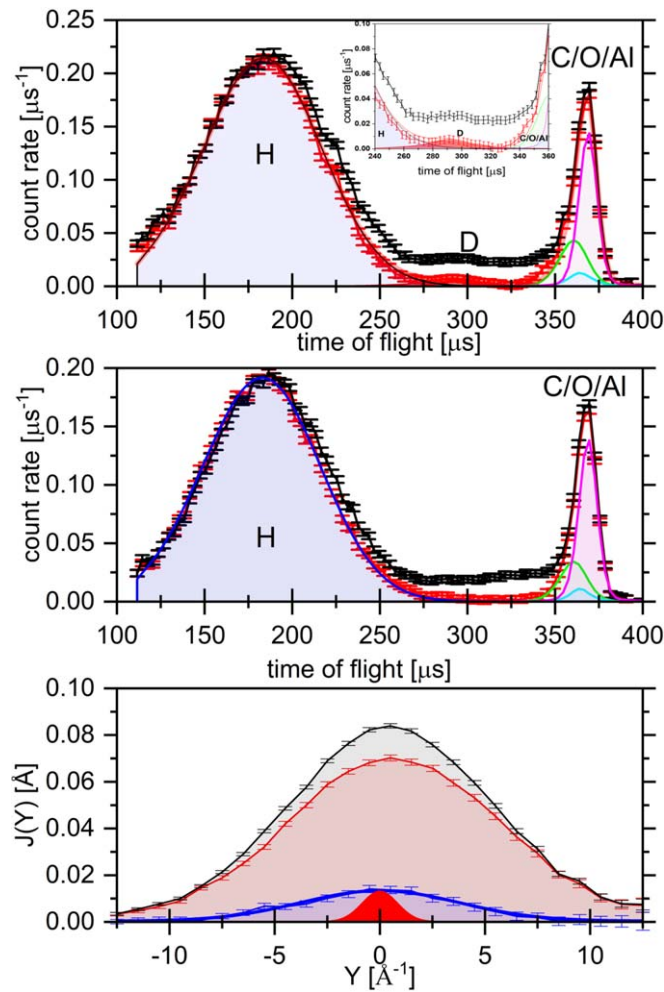
Figure 2. Top and middle panels: the raw (black line and points with error bars) and the corrected (red line and points with error bars) d-isopropanol (top panel) and isopropanol data (middle panel); the fitting curve of the total, corrected TOF NCS data (solid red line), together with the fitting lines for the individual recoil peaks (thick solid lines) of the hydrogen (black), deuteron (red—top panel only), carbon (green), oxygen (cyan), and aluminium (magenta). Top panel inset: the close-up of the top panel showing the TOF data region of the deuteron recoil peak together. Bottom panel: the hydrogen longitudinal momentum distribution in isopropanol (black line and data), the hydrogen in d-isopropanol, scaled by 7/8 (red line and data), and their difference (blue line and data) together with the fitting curve (solid blue line) and the hydrogen resolution function in the longitudinal momentum space (solid red area). See text for details.

increasing the number of events [24]. In practice, already one million individual neutron histories propagated through the Monte-Carlo simulation produces practically noiseless signals [24] . Moreover, the errors of the fitting parameters (peak widths and intensities) almost do not propagate through the gamma-background and multiple-scattering corrections, largely owing to the fact that they result from integration-type of calculations [24, 46]. In practice, the shapes of both types of corrections do not change within the two standard deviations of the uncertainties of the fitting parameters, which is tantamount to the iterative approach to TOF NCS data correction and fitting [24, 46].

The coloured solid lines in the top and middle panel of figure 2 represent the fitting curves of the fitting curves calculated using the expression for the total count rate for TOF NCS data (given by Eg. (1)), as well as the fitting curves representing contributions of recoil peaks of individual masses to the total count rate. As mentioned in point 2 of the TOF NCS data treatment protocol described above, the fitting curves were computed using the stoichiometrically fixed relative peak intensities. The technique of stoichiometric fixing is a potent tool in fitting TOF NCS data as it enhances the precision of the determination of the recoil peak widths being the only non-linear fitting parameters of the model given by Eg. (1). Importantly in the context of the determination of the NMD widths and kinetic energy values of deuteron, the stoichiometric fixing greatly improves the precision of the determination of the width of the deuteron NMD. When averaged over results obtained from all forward scattering detectors, the uncertainty of the deuteron NMD width does not exceed 0.2 Å^{-1}, and this value will be used hereinafter as an upper conservative bound.

The bottom panel in figure 2 shows the longitudinal momentum distribution of the hydrogen in isopropanol, the hydrogen in d-isopropanol, and their difference, representing the longitudinal momentum distribution of the hydrogen in the OH group, together with the fitting curve and the hydrogen resolution function in the longitudinal momentum space. The longitudinal momentum distribution of the hydrogen has been scaled by the factor of 7/8 in order to account for a different number of protons in isopropanol and d-isopropanol. It is worth noting that this scaling can only be performed in the longitudinal momentum space of the proton, not in the TOF domain. The reason for this is that the TOF NCS spectra contain only the information about the relative number of moles of the constituent nuclear species per formula unit of the sample (see equation (1)). Thus, a subtraction of a normalised and scaled TOF NCS spectrum of d-isopropanol from the normalised TOF NCS spectrum of isopropanol would inevitably lead to a creation of a negative residual signal in the TOF region of the deuteron recoil peak and a positive residual signal in the TOF region of the carbon, oxygen, and aluminium recoil peaks. In other words, one cannot apply a single scaling factor to the entire TOF NCS spectrum in order to isolate the TOF NCS contribution from the hydrogen in the OH group of the isopropanol. Such operation must be performed after the recoil peak isolation (subtraction of the recoil peaks of all other nuclear species apart from the hydrogen) in the TOF domain. Moreover, the isolated in the TOF domain proton recoil peaks in isopropanol and d-isopropanol correspond to different scattering angles and thus are not centred at the same TOF values, thus rendering the peak subtraction less precise an operation. Thus, focusing on the proton longitudinal momentum space followed by peak subtraction in the same space seems like the most numerically stable and precise option.

Finally, let us mention that the longitudinal momentum distribution of the OH group proton, illustrated as a solid blue line in the bottom panel in figure 2, can be fitted in a more reliable, robust, and precise manner owing to the signal differencing procedure outlined above. Namely, all signal fluctuations other than random Poissonian noise that is present in both longitudinal momentum distributions of isopropanol and d-isopropanol cancel out in this differencing procedure. This is clearly seen in the data shown in the region of longitudinal momentum magnitudes between 5 and 10 inverse Angstroms, on the right-hand side of the bottom panel in figure 2. The resultant difference-curve is then much smoother and more regular, resulting in more precise values of the fitted parameters. Moreover, the resolution function for the measurement of the proton longitudinal momentum distribution (red solid area in the bottom panel of figure 2) is much narrower than in the case of other nuclear mass-dependent VESUVIO resolution functions [8, 10–12, 47, 48], thus enabling high-precision work. Taken together, data focusing and high-resolution longitudinal nuclear momentum distribution spectroscopy yield widths of proton momentum distributions in isopropanol and d-isopropanol with the precision better than 0.2 inverse Angstrom. Thus, a value of 0.2 inverse Angstrom will be hereafter used as an upper conservative bound.

3. Results and discussion

As a first step in the interpretation of the values of the recoil peak widths, obtained from the NCS experiments, an *ab initio* calculation was performed. Two sets of simple *ab initio* calculations with the Density Functional Theory (DFT) method B3LYP using the basis set B3LYP/6–31 g* using Gaussian 98, revision A11, were performed in the limit of a single isolated molecule: (i) in vacuo calculation, and (ii) a calculation in a solvent environment of water. In the latter case, the solvent was modelled by placing the molecule within the solvent reaction field. For this, the self-consistent reaction field (SCRF) methodology, implemented using the COnductor-like Screening MOdel (COSMO) variant [49] of the CPCM model [50], was applied. COSMO is a variant of the continuum solvation models, which uses a scaled conductor boundary condition instead of the much more complicated dielectric boundary condition for the calculation of the polarization charges of a molecule in a continuum. The optimisation procedure led to a stable configuration and no imaginary frequencies.

Table 1 shows the predictions for the isotropic average values of the widths of the proton, carbon and oxygen momentum distributions in isopropanol based on the DFT calculation *in vacuo* and the calculation in a solvent environment of water. Table 2 shows the results of the analogical calculation for d-isopropanol, also including the value for D in the OD group. First, as an aside, it is worth noting that, in the case of the carbon, oxygen, and deuteron, the above theoretical predictions encourage the conclusion that, in principle, the NCS method is capable of achieving site and solvent selectivity in the idealised case of nearly-perfect resolution.

Taking into account, however, that the single-standard deviation (1-STD) error-levels of the present measurements of the widths of C and O momentum distributions are around 0.7–0.8 Å^{-1}, this remains still in the realm of the future vision for the much-needed upgrade of the NCS technique. Thus, site-selective isotopic substitution remains at present the only plausible route to achieving site-selectivity of the NCS method beyond the proton, a realisation that motivated this work.

Table 1. Predictions for the isotropic average values of the widths of the proton momentum distributions in isopropanol based on the DFT calculation *in vacuo* and the calculation in a solvent environment of water.

Atom no.	Atom label	σ [Å^{-1}]			
		T = 250 K		T = 300 K	
		in vacuo	in water	*in vacuo*	in water
1	C	12.4	12.3	12.7	12.6
2	C	13.1	13.1	13.3	13.3
3	C	12.4	12.3	12.7	12.5
4	O	12.0	11.9	12.5	12.4
5	H	5.0	5.0	5.1	5.0
6	H	5.0	5.0	5.0	5.0
7	H	5.0	5.0	5.0	5.0
8	H	5.0	5.0	5.0	5.0
9	H	5.1	5.1	5.1	5.1
10	H	5.0	5.0	5.0	5.0
11	H	5.0	5.0	5.0	5.0
12	H	5.0	5.0	5.0	5.0

Table 2. Predictions for the isotropic average values of the widths of the proton momentum distributions in d-isopropanol based on the DFT calculation *in vacuo* and the calculation in a solvent environment of water.

Atom no.	Atom label	σ [Å^{-1}]			
		T = 250 K		T = 300 K	
		in vacuo	in water	*in vacuo*	in water
1	C	12.3	12.2	12.5	12.5
2	C	13.0	13.1	13.1	13.3
3	C	12.4	12.3	12.7	12.6
4	O	12.2	12.2	12.7	12.7
5	D	6.1	6.0	6.1	6.0
6	H	5.0	5.0	5.0	5.0
7	H	5.0	5.0	5.0	5.0
8	H	5.0	5.0	5.0	5.0
9	H	5.1	5.1	5.1	5.1
10	H	5.0	5.0	5.0	5.0
11	H	5.0	5.0	5.0	5.0
12	H	5.0	5.0	5.0	5.0

The main observation from the DFT calculation mentioned above is that, unlike for carbon, for hydrogen, the DFT-predicted values, both *in vacuo* and in the presence of the water solvent model, are almost independent on the position of the hydrogen atom in the molecule. Treating the sets of these values as distributions, one can conclude that the standard deviations of these distributions amount to less than 1% of their mean values. This is an encouraging result, bearing in mind that NCS is not site-selectively measuring the proton momentum distributions. It means that in this particular case one can compare the widths of proton momentum distributions from NCS experiments with doubly-averaged (first over directions in space for each individual type of proton, and then over different types of protons in the molecule) theoretical predictions. Thus, one can assume that any discrepancy between the average theoretical prediction and the experimental value must signal a failure of the harmonic approximation to account for the local-effective potentials experienced by all protons in isopropanol and d-isopropanol. In what follows, our discussion about the degree of anharmonicity in both molecular systems will be motivated by this notion.

Figure 3 shows the values of the widths of nuclear momentum distributions of H in isopropanol, H in d-isopropanol, and D in d-isopropanol, obtained from fitting Gaussian profile functions to recorded NCS data, as well as the theoretical predictions for the average H and D widths, based on the harmonic *ab initio* DFT *in vacuo* calculation and the calculation in a solvent environment of water.
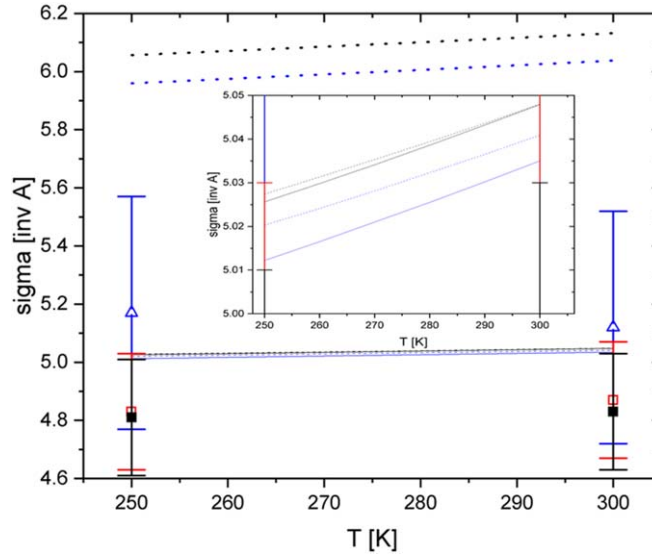
Figure 3. The values of the widths of nuclear momentum distributions of H in isopropanol (black filled squares), H in d-isopropanol (red open squares), and D in d-isopropanol (blue open triangles), obtained from fitting Gaussian profile functions to recorded NCS data. The theoretical predictions for the average values of the widths of H and D momentum distributions, based on the *ab initio* DFT *in vacuo* calculation and the calculation in a solvent environment of water are shown in the main figure and the inset as: (i) solid black and blue lines for the average H width in isopropanol *in vacuo* and in water solvent calculation, respectively; (ii) dashed black and blue lines for the average H width in d-isopropanol *in vacuo* and in water solvent calculation, respectively, and (iii) dotted black and blue lines for the D width in OD in d-isopropanol *in vacuo* and in water solvent calculation, respectively.

As mentioned above, in the case of H in isopropanol and d-isopropanol both the experimental values and the theoretical predictions are for the values averaged about all proton types in the molecules, reflecting the mass-resolved and site-averaged nature of the NCS measurements of the hydrogen momentum distributions. However, in the case of the D momentum distribution measurement in d-isopropanol, the NCS is effectively site-selective as there is only one type of D sites in this molecule, corresponding to D in the OD group. Clearly, all the experimental values shown in figure 3 are systematically below their respective DFT predictions, calculated within the harmonic approximation (HA). Moreover, the viral theorem predicts, in the case of pronounced anharmonicity of the local effective potential experienced by the nuclei, that the average nuclear kinetic energy becomes less than half of the total energy of the particle confined in the potential [51]. Taken together, the results shown in figure 3 signal a failure of the harmonic approximation to account for the local-effective potentials experienced by all protons in isopropanol and d-isopropanol.

The next step in our appraisal of the local effective potential experienced by H and D in isopropanol and d-isopropanol is summarised in figure 4. The top panel of figure 4 shows the ratios of the kinetic energies of H in OH in isopropanol and D in OD in d-isopropanol, obtained from the widths of NMDs using the expression:

$$\frac{E_{kin,H}}{E_{kin,D}} = \frac{\dfrac{3\hbar^2\sigma_H^2}{2M_H}}{\dfrac{3\hbar^2\sigma_D^2}{2M_D}} \tag{3}$$

where M_H and M_D are masses of H and D in amu and the Planck constant is $\hbar = 2.04 \ \mathrm{meV}^{0.5} \ \mathrm{amu}^{0.5} \ \text{Å}$.

It is worth noting that, by virtue of error propagation, the error of the ratio of the kinetic energies given by Eg. (3) can be written as:

$$\Delta\left[\frac{E_{kin,H}}{E_{kin,D}}\right] = \frac{M_D}{M_H}\sqrt{\frac{\sigma_H^2 \Delta\sigma_H^2}{\sigma_D^4} + \frac{\Delta\sigma_D^2}{\sigma_D^2}} \tag{4}$$

where $\Delta\sigma_H$ and $\Delta\sigma_D$ are one- standard deviation (1-STD) error of the values of the widths of the proton and deuteron momentum distributions, σ_H and σ_D, respectively. The bottom panel of figure 4 shows the values of the 1-STD errors of the ratio given by equation (3), simulated for the average value of σ_H and σ_D from figure 3 and the values of $\Delta\sigma_H$ and $\Delta\sigma_D$ of 0.2 and 0.4 inverse Angstrom, respectively. It is worth noting that, for the values of the 1-STD errors, $\Delta\sigma_D$ in the range of 0.4 inverse Angstrom, the ratio of the kinetic energies of the hydrogen and deuteron is capped by the value of 0.2. Thus, in our further discussion we will use the value of 0.2 as an upper conservative bound for the 1-STD error, $\Delta\left[\frac{E_{kin,H}}{E_{kin,D}}\right]$.
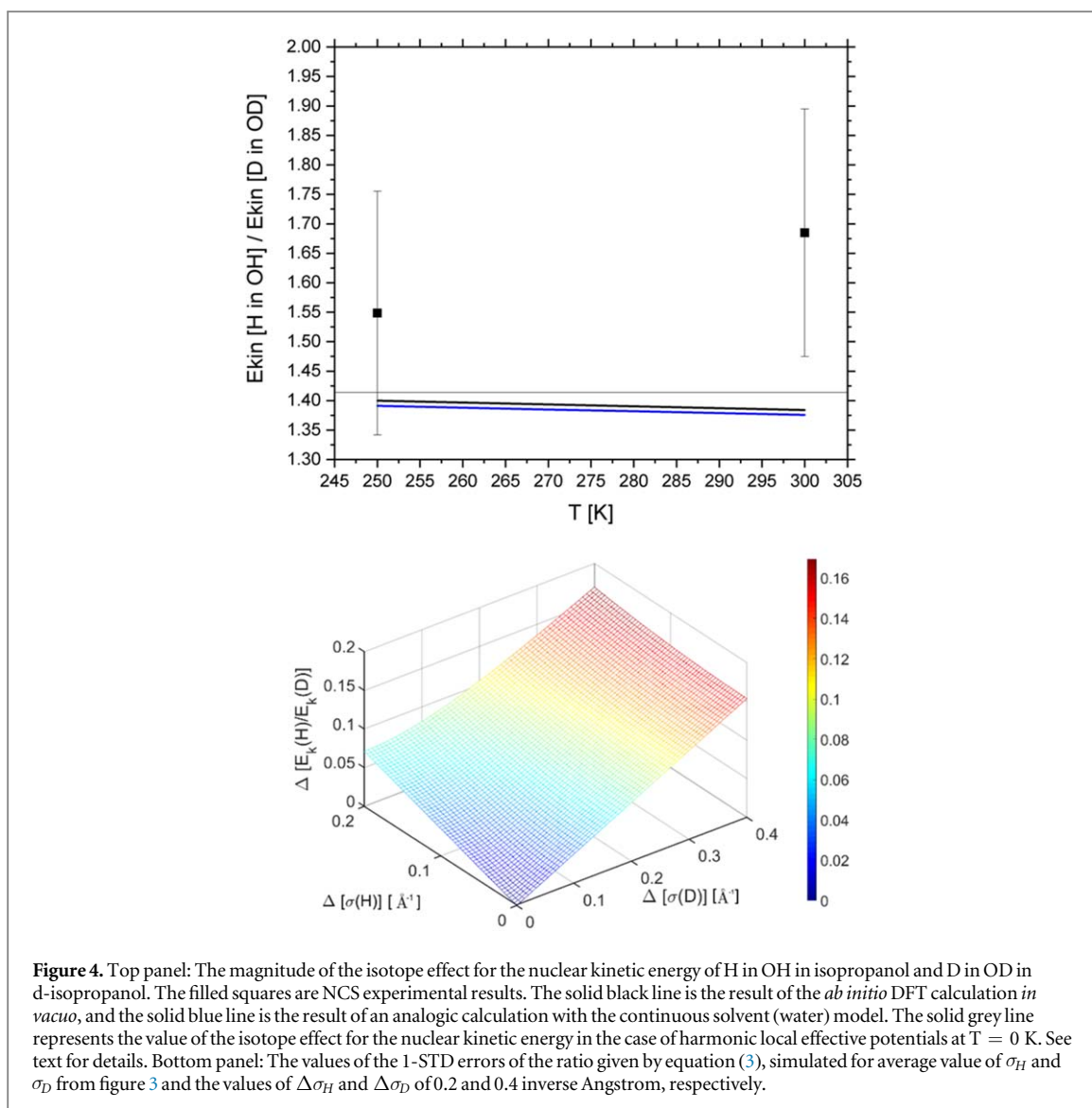
Figure 4. Top panel: The magnitude of the isotope effect for the nuclear kinetic energy of H in OH in isopropanol and D in OD in d-isopropanol. The filled squares are NCS experimental results. The solid black line is the result of the *ab initio* DFT calculation *in vacuo*, and the solid blue line is the result of an analogic calculation with the continuous solvent (water) model. The solid grey line represents the value of the isotope effect for the nuclear kinetic energy in the case of harmonic local effective potentials at T = 0 K. See text for details. Bottom panel: The values of the 1-STD errors of the ratio given by equation (3), simulated for average value of σ_H and σ_D from figure 3 and the values of $\Delta\sigma_H$ and $\Delta\sigma_D$ of 0.2 and 0.4 inverse Angstrom, respectively.

In figure 4 the experimental values of $\left[\frac{E_{kin,H}}{E_{kin,D}}\right]$ are contrasted with predictions from the harmonic DFT calculation performed in vacuo and with the continuous solvent (water) model, taking into account the Boltzmann population factors for different modes of vibrations projecting onto H in OH in isopropanol and D in OD in d-isopropanol.

Additionally, the value of the isotope effect for the nuclear kinetic energy in the case of harmonic local effective potentials experienced by H and D, calculated at T = 0 K, is shown in figure 4 as a constant solid line and represents a result from the theory of the quantum harmonic oscillator:

$$\frac{E_H}{E_D} = \frac{m_D}{m_H}\left(\frac{\sigma H}{\sigma D}\right)^2 = \frac{m_D}{m_H}\left(\frac{mH}{mD}\right)^{1/2} = \left(\frac{mD}{mH}\right)^{1/2} = 1.41 \tag{5}$$

It is worth noting that the theoretical ratio plotted in figure 4, Ekin(H in OH)/Ekin(D in OD), was *not* taken to be the ratio of the *reduced* masses of D in OD and H in OH, being 1.373. The reason for that is that the NCS method is probing the *total* nuclear kinetic energies *not* the energies of the individual modes of vibration of the nuclei. The total nuclear kinetic energies are functions of the Boltzmann-population-weighted first-moments of the atom-projected VDOS distributions. These quantities are in turn calculated taking the masses of the freely recoiling nuclei within the Impulse Approximation. Physically, the values of these masses are given by the conservation of the total kinetic energy and momentum of the system consisting of an impinging neutron and a target nucleus that recoils after the collision with the neutron during the Compton scattering event. Mathematically, the conservation of the nuclear kinetic energy and momentum during a Compton event is reflected in the fact that the longitudinal momentum distributions of all nuclear species are centred at the values of zero. This fact is clearly seen in the bottom panel of figure 2 for H in OH. The centre of the longitudinal

momentum distribution for the proton in the OH group in this figure corresponds to the zero value of the longitudinal momentum as calculated for the value of the freely recoiling proton of the mass of 1.0079 amu. For the case of D in OD, the same property is reflected in the fact that the TOF NCS data treatment of the recoil peaks of D in d-isopropanol always results in the recoil peak positions in the TOF domain that correspond to the value of zero longitudinal nuclear momentum of the freely recoil mass of D, i. e., 2.015 amu (see the top panel in figure 3). The physical picture pertaining to the momentum distributions of H in OH and D in OD is thus that they both correspond to the distributions of all nuclear momentum components of all modes of vibrations that have non-zero contributions to the motions of H in OH and D in OD functional groups. Although the bulk of contributions to these distributions comes from the nuclear stretching modes, there are also non-negligible contributions from other modes of vibrations, such as bending modes for example. Thus, there is no single effective mode of vibration and a single values of effective mass pertaining to this mode that is representative for the nuclear motion of H in OH and D in OD. In other words, the effective mean forces acting on of H in OH and D in OD are not aligned along the directions of the OH and OD bond respectively but rather reflect complicated interplays between all vibrational modes.

It is worth noting that, the theoretical predictions taking into account Boltzmann population factors yield kinetic energy isotope effect that is decreasing with increasing temperature. This is the reflection of the fact that, as temperature increases, the high-energy vibrational modes contributing to the motion of D in OD are being populated faster than the modes in the case of H in OH. In consequence, the temperature-weighted mean values of the atom-projected vibrational densities of states (and thus the average kinetic energy values) shift towards higher energies faster in the case of D in OD. In other words, the trends represented by solid black and blue lines, when extrapolated to T = 0 K, would reach the value of 1.41. As an aside, we remark that an interesting solvent effect is clearly visible in theoretical prediction depicted in figure 3. Namely, the presence of the solvent (water) seems to shift the theoretical prediction towards lower magnitudes, as compared to the prediction *in vacuo*. This indicates that, unlike the absolute values of the nuclear kinetic energy for H and D, the site-selective values of the magnitude of the isotope effect for the kinetic energies can potentially be used as observables of choice for the detection of solvent-induced nuclear quantum effects. Of course, this observation is of preliminary character and needs further confirmations by means of more sophisticated *ab initio* methodology (e. g., *ab initio* molecular dynamics or simulations). Notwithstanding the last remark, a clear departure is visible in figure 4 for the NCS data from the harmonic approximation results. Firstly, the experimental values are placed systematically higher than any harmonic vibration prediction. Secondly, the temperature trend for the experimental data is opposite as compared to the theoretical predictions. This result further corroborates the notion of the anharmonic character of the local-effective potentials of H in OH in isopropanol and D in OD in d-isopropanol in the condensed phase.

Further insight into the possible shape of the local effective potential experienced by H in OH and D in OD in condensed phases of isopropanol and d-isopropanol can be gained owing to the analysis of trends visible is spectroscopic measurements for systems with hydrogen bonds, performed by McKenzie *et al* [52]. The first observation is that the magnitudes of the isotope effect for the nuclear kinetic energy, observed in our NCS experiments, are well within the range of values observed for the longitudinal O–H(D) stretching mode for hydrogen to deuteron isotopes is observed experimentally, varying from 0.85 to 2.0 [52–55]. In contrast, for the torsional/bending modes, the isotope effects are consistent with the semi-classical harmonic ratio of 1.41 [52–55]. Thus, the vibrational frequency isotope effect is expected to correlate well with the nuclear kinetic energy isotope effect for H(D) in hydrogen bonds like those formed by H(D) in OH (OD) in isopropanol and d-isopropanol. Both systems investigated here belong to the class of weakly hydrogen-bonded systems. Unlike the nearly harmonic weak hydrogen bonds, moderate to weak hydrogen bonds are anharmonic at the bottom of their effective BO potential energy curve. This type of anharmonicity can be very well parametrised using the Morse potential [52]. The Morse potential energy function is of the form:
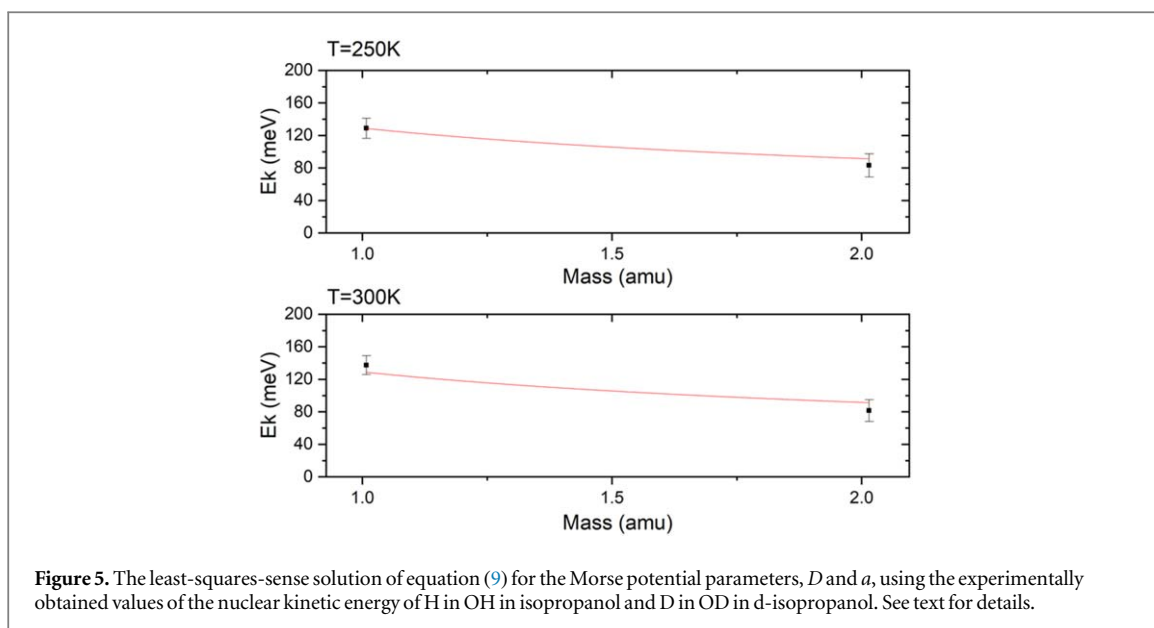
$$V(r) = D(1 - e^{-a(r-r_e)})^2 \tag{6}$$

where r is the distance between the atoms, r_e is the equilibrium bond distance, D is the potential well depth (defined relative to the dissociated atoms), and a is the attenuation length that controls the width of the potential. The Morse potential, rather than being defined by equation (6), is often rewritten in a form in which the zero of the potential energy is shifted down by subtracting the value of the dissociation constant D, which gives:

$$V(r) = D(1 - e^{-a(r-r_e)})^2 - D = D(e^{-2a(r-r_e)} - 2e^{-a(r-r_e)}) \tag{7}$$

The Eigen energies of the Schrodinger equation with the Morse potential can be written in terms of its original variables as:

$$E_n = \hbar a \sqrt{2D/M}(n + 1/2) - [\hbar a \sqrt{2D/M}(n + 1/2)]^2/4D \tag{8}$$

Figure 5. The least-squares-sense solution of equation (9) for the Morse potential parameters, D and a, using the experimentally obtained values of the nuclear kinetic energy of H in OH in isopropanol and D in OD in d-isopropanol. See text for details.

Assuming that in our systems the degree of the departure from the harmonicity is small and that one can still use the result of the virial theorem stating that the average kinetic energy of a nucleus in the potential of a weak hydrogen bond amounts to half its total energy, $E_{kin} = \frac{1}{2} E_0$, one obtains the following formula for the nuclear kinetic energy of a nucleus of mass M in the Morse potential:

$$E_{kin,Morse} = \sqrt{a^2\hbar^2/16M}\sqrt{2D} - a^2\hbar^2/16M \qquad (9)$$

Consequently, the magnitude of the kinetic energy isotope effect for the Morse potential can be expressed as [52]:

$$E_{kin,Morse}(H)/E_{kin,Morse}(D) = \sqrt{2}((1 - 2\sqrt{a^2\hbar^2/8MD})/(1 - \sqrt{2}\sqrt{a^2\hbar^2/8MD})) \qquad (10)$$

Interestingly, using equation (10), one can obtain the upper and lower conservative bounds for the magnitude of the kinetic energy isotope effect that can possibly stem from the Morse potential. Noting that the combination of the Morse potential parameters given by $\sqrt{a^2\hbar^2/8MD}$ must always yield positive values, the values of $E_{kin,Morse}(H)/E_{kin,Morse}(D)$ are bounded from below by $E_{kin,Morse}(H)/E_{kin,Morse}(D) = 2$ (for the asymptotic condition, $\sqrt{a^2\hbar^2/8MD} \to \infty$), and, for $\sqrt{a^2\hbar^2/8MD} \to 0$, from above by $E_{kin,Morse}(H)/E_{kin,Morse}(D) = \sqrt{2}$. Thus, the set of two inequalities given by $E_{kin}(H)/E_{kin}(D) < \sqrt{2}$ or $E_{kin}(H)/E_{kin}(D) > 2$ can be thought of 'selection rules' for the Morse potential, in as much as the relation $E_{kin}(H)/E_{kin}(D) = 1.41$ is the 'selection rule' for the harmonic potential. In practice, however, even for large anharmonicity ($\sqrt{a^2\hbar^2/8MD} \sim 0.2-0.25$), the ratio $E_{kin,Morse}(H)/E_{kin,Morse}(D)$ only decreases from the harmonic limit to about 1.1–1.2 [52]. Taking into account the selection rules developed above for the case of the Morse potential, the values of the magnitudes of the isotope effect shown in figure 4 would signify that the local effective potential experienced by H in OH and D in OD in both alcohols under investigation are not consistent with the assumption that the underlying potential is of the Morse type. However, if one takes into account the 1-STD errors of the experimental values of the magnitudes of the isotope effect, being of the order of 0.2, the experimental values do fall within the range of values allowed for the harmonic and Morse potentials. Mathematically, one cannot solve exactly equation (9) using the mean experimental values of the kinetic energies of H in OH and D in OD. One can, however, solve this equation in a least-squares-sense taking into account 1-STD errors of the measured kinetic energy values. This procedure is summarized graphically in figure 5. Treating the nuclear mass M as a continuous variable one can graphically solve equation (9) by finding the values of the parameters of the Morse potential, D and a, that solve this equation for the given (known from the NCS experiment) values of $E_{kin}(M_H)$ and $E_{kin}(M_D)$, taking into account the 1-STD errors of $E_{kin}(M_H)$ and $E_{kin}(M_D)$. This procedure is shown in figure 5 for two temperatures, at which NCS were performed, T = 250 K and T = 300 K. Assuming a and D fulfil equation (9) at both T = 250 K and T = 300 K, we obtain $a = 2.2 \pm 0.2\ \text{Å}^{-1}$ and $D = 6713 \pm 515$ meV. Interestingly, the obtained values of a and D fall within the range of Morse potential parameters tabulated in the literature for simple molecular systems [56].

In the last step of our appraisal of the local-effective potential experienced by H in OH in isopropanol, we calculate the degree of the delocalisation in space and momentum of the muoniated variant of the isopropanol. We start by noting that it is plausible to assume that the Born–Oppenheimer approximation (BOA) is valid for

the case of H, D, and Mu-substituted molecular species. The reasons to assume this are twofold. Firstly, the assumption of the validity of the BOA and the lack of non-adiabatic effects have already been tested both theoretically [57] and experimentally [58, 59] for the case of the neutron Compton scattering on lightweight nuclei. Mathematically, the theory predicts that the BOA violation in NCS would be reflected in a build-up of satellite peaks at the low-energy transfer shoulders of the main recoil peaks (that are present in the ideal case of the absence of non-BOA effects) [57]. Such non-BOA effect would be most pronounced in the case of lightweight nuclei [57]. In the longitudinal momentum distribution domains, such non-BOA effects would have led to shifts of the centroids of nuclear longitudinal momentum distributions of H and D towards lower values of the longitudinal momentum [57]. However, no such effects have been experimentally observed in the NCS spectroscopy [58, 59]. Such is the case also for the nuclear momentum distributions of H in isopropanol and D in d-isopropanol discussed in this work. Namely, no additional shifts of the centroids towards lower values of the longitudinal nuclear momentum have been observed here during the NCS data treatment described above.

When the hydrogen is substituted by a positive muon, the nucleus-to-electron mass ratio falls from a value of 1836.15 to 206.77 with the resulting atom muonium, Mu, behaving like a light isotope of hydrogen [60]. One could anticipate that for muonium-substituted molecules, the isotope effect is so large that the BOA is invalid. However, non-adiabatic and non-BOA effects are extremely small as observed by the muon-spin resonance and predicted by theoretical calculations for Mu-substituted molecular species and solid-state defect centres, at least in their ground electronic states [61]. For example, for isotopomers of the hydrogen molecule Webster and McKenna showed, by a series of non-adiabatic calculations beyond the Born–Oppenheimer approximation, that the key isotope effect arises through the mass dependence of the zero-point vibrational energy but essentially the same single potential-energy curve underlies the nuclear dynamics of all nuclear isotopic species [62]. On the whole, this result indicates the so-called *trivial* isotope effect, which, in order to be accounted for, in essence does not require resorting to non-adiabatic calculations. The reason for this is that the electronic structure for the protonic and muonic species is identical within the Born–Oppenheimer approximation, mass effects being manifest only through differences in zero-point vibrational motion and the alteration of the vibrational modes. A further theoretical study of the muonium-substituted species MuCO˙ and MuCO⁺ also points out on the trivial isotope effect being the mere consequence of the mass ratio of the isotopic species. It was namely indicated that the vibrational frequencies of the C–Mu bond in the radical MuCO˙ increase by a factor close to a value of three, as expected for harmonic vibrations where the frequency varies inversely with the square root of the reduced mass for a Mu–C bond [63]. Furthermore, another study of vibrational behaviour of the carbon-muonium bond in the muoniated ethyl radical points out that, despite the great disparity in mass of the hydrogen and muonium isotopomers, the mere effect of the isotopic substitution is that the zero-point vibrational level lies significantly higher on the potential surface for Mu and the C–Mu bond executes large amplitude vibrations compared with a C–H bond, with the mean-square displacement for the C–Mu bond being three-time larger than the figure for the C–H bond [60]. However, using the relation between the magnitude of the force constant acting on the nuclear species in a bond, the magnitude of the mean-square displacement and the value of the zero-point energy for the stretching mode of the C–H bond, the authors arrive at the conclusion that values of the equilibrium stretching force constant are essentially isotope independent, despite the fact that the C–Mu bond executes large-amplitude vibrations and the zero-point vibrational energy of C–Mu is large compared with a C–H bond [60]. Using the language of the NCS one could thus state that the effective mean forces acting on Mu in the C–Mu bond and H in the C–H bond and their respective potentials are essentially the same. This is a significant observation as it essentially lies at the foundation of the so-called *steric* isotope effect [60]. Namely, the isotopic substitution introduces overcrowding if, as is supposed, a muonium atom has a larger steric requirement than hydrogen [60]. The energetic consequence of the steric isotope effect is that there is an isotopic shift, induced by steric interaction, in the zero-point vibrational energy [60].

Taken together, the experimental and theoretical results discussed above point out that one can assume that muon and proton are governed by almost identical potential-energy surfaces in analogous species [61]. Moreover, the notion of the equilibrium or Born–Oppenheimer structure can be used in the above considerations as a benchmark for the estimate of the magnitude of the isotope effect as long as the BOA is considered valid in the muoniated radicals. Importantly, the BOA leads to a potential energy surface that is a function of nuclear positions but not of nuclear masses. The validity of the BOA for Mu-substituted molecules has often been questioned on the qualitative level. However, as we have seen in the discussion in the last few paragraphs, the quantitative theoretical assessments lead to the conclusion that the departure from the BOA manifests as an increase in force constant confining the muon of not more than a few per cent. The effect on observable molecular properties, such as the vibrational frequencies, root-mean-square displacements and the widths of nuclear momentum distributions, varying as $\sqrt{k/m}$, $(mk)^{-1/4}$ and $(mk)^{1/4}$ respectively, are likely to be very small [61]. Thus, the isotope effects are primarily due to zero-point energy in the ground vibrational state.

Assuming that both hydrogen and Mu in OH in isopropanol experience the same Morse potential, one can calculate the kinetic energies of both particles according to equation (9). Taking the parameters of the potential as $a = 2.2$ Å^{-1} and $D = 6713$ meV, one gets $E_{kin,Morse}(H)/E_{kin,Morse}(Mu) = 0.34$, thus a value higher than one third, assumed in the case of the harmonic approximation and also a result typical for the Morse potential [61]. Using the definition of the kinetic energy (equation (3)) and assuming that the width of the proton momentum distribution in OH is 4.7 Å^{-1}, we get the prediction for the width of the Mu momentum distribution of 2.7 Å^{-1}. Inverting between the width of the momentum and spatial delocalisation (using the Heisenberg uncertainty principle for Gaussian wave packets), we get the prediction for the extent of the spatial delocalisation of the Mu in the muoniated isopropyl radical of 0.37 Å.

It is tempting to put our estimates of the kinetic energy, space and momentum delocalisation of the Mu in isopropyl alcohol in the context of the literature results on nuclear quantum and spin dynamics of Mu in condensed matter. Mu, when embedded in solid-state systems is usually shown to be dominated by the tendency to form bonds with adjacent atoms. For example, for Mu in silicon the values of the zero-point energy are, depending on its position between the two Si atoms in the lattice, between 240 and 270 meV, for the motion along the bond direction, and between 540 and 560 meV when the motion perpendicular to the bond is included [64]. These amounts of zero-point energy are sufficient to place the average position of the muon at the silicon-silicon bond centre. However, because of the extraordinary light mass of the muon, the inclusion of the zero-point motion expands the bond by 0.88 Å. Moreover, if one replaces the muon with a proton the corresponding extension is about 0.86, and 0.84 Å for the deuteron [64]. From our estimates we are unable to predict the magnitude of the hydrogen bond extension in the muoniated isopropyl. We can, however, assess the amount of the zero-point energy of the Mu. Taking the kinetic energy of the proton in OH in isopropanol as 132.5 meV at T = 300 K and scaling it by 1/0.34 we obtain an estimate of 389.8 meV for the kinetic energy and 779.6 meV for the zero-point energy of the Mu in the muoniated isopropanol at the same temperature. This value is ca. 40% larger than the value reported for the Mu in the silicon lattice. Thus, one can anticipate that this amount of the zero-point energy may elongate the hydrogen bond in the muoniated isopropyl beyond the value of 0.88 Å.

The magnitude of the zero-point energy can also be used to predict the transition from the classical to the quantum diffusion regime of Mu in solid-state systems. It is predicted that the transition between the classical and quantum Mu diffusion takes place at a temperature $T^* \sim \nu_0$, where ν_0 is the vibrational frequency of the particle in its potential well [65]. For example, for Mu atoms in crystals, T^* can be estimated to be on the order of several hundred Kelvin [66, 67]. Inspired by this result, we can provide an upper conservative bound for the temperature corresponding to the onset of the classical hopping of the Mu in the isopropyl in the liquid phase at ambient conditions. Our estimate that the magnitude of the zero-point energy of the Mu in the liquid isopropanol is of the order of ca. 9000 K and 188.4 THz, respectively, 2 orders of magnitude more than the values reported for solids. Thus, quantum diffusion of the Mu is much more likely at ambient conditions in the liquid isopropanol than in many solid-state systems.

Last but not least, the isotope effects on the zero-point energy between Mu, hydrogen, and deuteron in molecular and solid-state systems are widely discussed in the context of the validity of the predictions for the magnitudes of the hyperfine coupling constants in μSR work [61], a discussion that originally motivated the NCS work presented here. As a starting remark it is worth noticing that the classical or equilibrium structures of different isotopomers of the same system would be the same in the Born–Oppenheimer approximation, leading to identical equilibrium bond-lengths and identical spin density on deuteron, proton or muon, with their hyperfine constants scaling according to their gyromagnetic ratios [61]. However, experimentally this is not the case, both for rigid or more flexible molecules, a natural consequence of the different zero-point energies for muon and proton, and deuteron [61]. The relatively rigid structures of C60X (the monohydride isotopomers with X = D, H, Mu) provide a simple introduction to hyperfine isotope effects [61]. The influence of the different zero-point energies of the three isotopes on the magnitude of the hyperfine coupling is even more pronounced if the local-effective potential energy curve is anharmonic, such as the one describing D, H, Mu in C60X, which is very well approximated by the Morse potential [61]. Contrary to the harmonic case, there are now two main contributions to the isotope effect on the hyperfine coupling, the harmonic and the anharmonic one. Stretching and rocking modes as well as the motion transverse to the original double bond for C60X project on the motion of H and Mu differently. The net effect is that the position distribution of Mu is much more asymmetric and skewed towards the softer side of the potential than the position distribution of H. In such a scenario, the anharmonic contribution comes from the different average bond lengths and the harmonic contribution from the different root-mean-square excursions of H and Mu from the minimum of the potential energy surface [61]. In consequence, the different amounts of zero-point energy for H and Mu, equal to 220 and 590 meV respectively, are distributed in space completely differently, leading to completely different sampling by H and Mu of the unpaired electron spin density. One can imagine that, as the Mu bond is stretched to breaking point, hyperfine constants increase to the respective atomic values [61]. On the whole, the spin density on the deuteron, proton and muon is higher than the equilibrium-geometry value by 2%, 3% and 10%,

respectively, leading to overall isotope effects of 1% between C60D and C60H, and about 7% between C60H and C60Mu. Taking into account that our estimate of the zero-point energy of Mu in isopropyl is ca. 32% larger than the value for C60Mu, we can anticipate that the overall isotope effect for the hyperfine interaction between isopropyl and its muoniated counterpart is expected to be at least one third larger, i.e. in the region of 10%. Moreover, one can treat this estimate as lower conservative bound, as it assumes that the isopropyl is a rigid molecular system. However, in muoniated organic radicals with softer internal modes such as hindered rotations, hyperfine isotope effects can reach up to 20%. These large magnitudes of the isotope effects are mainly due to the averaging over bond angles (largely absent in the case of rigid molecules) and the role played by the soft modes [61].

We close our discussion by remarking that the estimates of the kinetic and zero-point energy, as well as the position and momentum delocalisation of the Mu in the muoniated isopropyl molecule in condensed phase is by no means an exact calculation, but merely a first step towards further elucidation of the nuclear and spin dynamics of Mu in this important system. One can imagine that, in the future, much more precise *ab initio* work, based for example on the PIMD approach, will be available. To this end, one can envisage a computational protocol in which our estimates are treated as additional constraints for the PIMD calculation, hopefully guiding it towards a much better agreement with experiment.

4. Summary

In this work, we have employed the combination of NCS and *ab initio* single-molecule vibrational calculation in order to perform a critical appraisal of the nuclear quantum dynamics of protons and deuterons in isopropyl and d–isopropyl in the condensed phase. Based on the classical results for the magnitude of the isotope effect for model inter-particle potentials, we were able to assess the degree of the isotope effect on nuclear and spin dynamics of Mu in muoniated isopropyl. The NCS technique has been employed for the first time as a tool shedding more light on the nuclear and spin dynamics of the Mu in the condensed phase. The obtained results can serve as conservative constraints for future precise *ab initio* calculations of properties of muoniated radicals in condensed matter systems and molecules.

Acknowledgments

ORCID iDs

Matthew Krzystyniak   https://orcid.org/0000-0003-0307-6871
Giovanni Romanelli   https://orcid.org/0000-0001-5963-4647

References

[1] Karlsson E B 1995 *Solid State Phenomena, As Seen by Muons, Protons, and Excited Nuclei* (Oxford: Oxford University Press)
[2] Blundell S J 1999 *Contemporary Physics* **40** 175-192
[3] Claxton A T and Graham A M 1998 *J. Chem. Soc., Faraday Trans.* **84** 121-134
[4] Roduner E, Strub W, Burkhard P, Hochmann J, Percival P W, Fischer H, Ramos M and Webster B C 1982 *Chemical Physics* **67** 275-285
[5] Webster B C and Buttar D 1992 *J. Chem. Soc. Faraday T.* **88** 1087-1092
[6] Oba Y, Kawatsu T and Tachikawa M 2016 *Journal of Chemical Physics* **145** 1-15
[7] http://isis.stfc.ac.uk/instruments/vesuvio/
[8] Andreani C *et al* 2014 Discussion: nuclear quantum dynamics - protons and beyond *J Phys Conf Ser* **571** 1-4
[9] Andreani C, Colognesi D, Mayers J, Reiter G and Senesi R 2005 Measurement of the momentum distribution of light atoms and molecules in condensed matter systems using inelastic neutron scattering *Advances in Physics* **54** 377–469
[10] Andreani C, Krzystyniak M, Romanelli G, Senesi R and Fernandez-Alonso F 2017 Electron-volt neutron spectroscopy: beyond fundamental systems *Advances in Physics* **66** 1–73
[11] Andreani C, Senesi R, Krzystyniak M, Romanelli G and Fernandez-Alonso F 2017 *Experimental Methods in the Physical Sciences* ed F Fernandez-Alonso and D L Price (New York: Academic) pp 403–57
[12] Andreani C, Senesi R, Krzystyniak M, Romanelli G and Fernandez-Alonso F F 2018 Experimental studies of nuclear quantum effects in condensed matter: the case of water *Rivista Del Nuovo Cimento* **41** 291–340
[13] Bermejo F J, Mompean F J, Srinivasan A, Mayers J and Evans A C 1994 Deep-inelastic neutron-scattering as a tool for the investigation of glassy dynamics *Physics Letters A* **189** 333–9
[14] Evans A C, Mayers J, Timms D N and Cooper M J 1993 Deep inelastic neutron-scattering in the study of atomic momentum distributions *Zeitschrift Fur Naturforschung section a-a Journal of Physical Sciences* **48** 425–32

[15] Mayers J 1990 Quantum effects in deep inelastic neutron-scattering *Phys Rev B* **41** 41–51

[16] Mayers J 1996 Measurement of atomic momenta in quantum fluids by high-energy neutron scattering *Journal of Physics-Condensed Matter* **8** 9423–7

[17] Mayers J 1997 Measurement of atomic momenta by high energy neutron scattering *Physica B* **234** 1186–8

[18] Mayers J, Reiter G F and Platzman P 2002 Measurement of proton momentum distributions by eV neutron scattering *Journal of Molecular Structure* **615** 275–82

[19] Reiter G F, Mayers J and Noreland J 2002 Momentum-distribution spectroscopy using deep inelastic neutron scattering *Phys Rev B* **65** 1–9

[20] Abdul-Redah T *et al* 2004 Recent developments of the e.VERDI project at ISIS *Physica B-Condensed Matter* **350** E837–40

[21] Andreani C, Colognesi D, Mayers J, Reiter G F and Senesi R 2005 Measurement of momentum distribution of light atoms and molecules in condensed matter systems using inelastic neutron scattering *Advances in Physics* **54** 377–469

[22] Fielding A L and Mayers J 2002 Calibration of the electron volt spectrometer, a deep inelastic neutron scattering spectrometer at the ISIS pulsed neutron spallation source *Nucl Instrum Meth A* **480** 680–9

[23] Mayers J and Adams M A 2011 Calibration of an electron volt neutron spectrometer *Nucl Instrum Meth A* **625** 47–56

[24] Mayers J, Fielding A L and Senesi R 2002 Multiple scattering in deep inelastic neutron scattering: Monte Carlo simulations and experiments at the ISIS eVS inverse geometry spectrometer *Nucl Instrum Meth A* **481** 454–63

[25] Mayers J and Reiter G 2012 The VESUVIO electron volt neutron spectrometer *Meas Sci Technol* **23** 1–18

[26] Mayers J, Tomkinson J, Abdul-Redah T, Stirling W G, Andreani C, Senesi R, Nardone M, Colognesi D and Degiorgi E 2004 VESUVIO-the double difference inverse geometry spectrometer at ISIS *Physica B-Condensed Matter* **350** E659–62

[27] Senesi R *et al* 2000 VESUVIO: a novel instrument for performing spectroscopic studies in condensed matter with eV neutrons at the ISIS facility *Physica B* **276** 200–1

[28] Krzystyniak M *et al* 2018 VESUVIO plus : the current testbed for a next-generation epithermal neutron spectrometer *J Phys Conf Ser* **1021** 1–4

[29] Romanelli G *et al* 2017 Characterisation of the incident beam and current diffraction capabilities on the VESUVIO spectrometer *Measurement Science and Technology* **28** 1-6

[30] Romanelli G, Rudic S, Zanetti M, Andreani C, Fernandez-Alonso F, Gorini G, Krzystyniak M and Skoro G 2018 Measurement of the para-hydrogen concentration in the ISIS moderators using neutron transmission and thermal conductivity *Nucl Instrum Meth A* **888** 88–95

[31] Santisteban J R, Granada J R and Dawidowski J 1999 *Physica B* **269** 345–55

[32] Damian J I M, Granada J R, Cantargi F and Roubtsov D 2017 New evaluation of thermal neutron scattering libraries for light and heavy water *EPJ Web of Conferences* **146** 1–3

[33] Dawidowski J, Granada J R and Blostein J J 2000 Neutron total cross-sections of normal and deuterated ethanol in the thermal and epithermal energy ranges *Nuclear Instruments & Methods in Physics Research section B-Beam Interactions with Materials and Atoms* **168** 462–6

[34] Dawidowski J, Santisteban J R and Granada J R 1999 Exploration of the dynamics of condensed matter through neutron total cross-section measurements *Physica B* **271** 212–22

[35] Romanelli G, Krzystyniak M, Senesi R, Raspino D, Boxall J, Pooley D, Moorby S, Schooneveld E, Rhodes N and Andreani C 2017 Characterisation of the incident beam and current diffraction capabilities on the VESUVIO spectrometer *Meas Sci Technol* **28** 1-6

[36] Farina J 1978 On the impulse approximation *Journal of Physics A: Mathematical and General* **11** 1915-1932

[37] Krzystyniak M and Abdul-Redah T 2010 Proton momentum distribution in solid and liquid HF *Phys Rev B* **82** 1-9

[38] Krzystyniak M, Adams M A, Lovell A, Skipper N T, Bennington S M, Mayers J and Fernandez-Alonso F 2011 Probing the binding and spatial arrangement of molecular hydrogen in porous hosts via neutron Compton scattering *Faraday Discussions* **151** 171–97

[39] Krzystyniak M, Druzbicki K and Fernandez-Alonso F 2015 Nuclear dynamics in the metastable phase of the solid acid caesium hydrogen sulfate *Phys Chem Chem Phys* **17** 31287–96

[40] Krzystyniak M, Druzbicki K, Romanelli G, Gutmann M J, Rudic S, Imberti S and Fernandez-Alonso F 2017 Nuclear dynamics and phase polymorphism in solid formic acid *Phys Chem Chem Phys* **19** 9064–74

[41] Jackson S, Krzystyniak M, Seel A G, Giggi M, Richards S E and Fernandez-Alonso F 2014 VESUVIO Data Analysis Goes MANTID *J. Phys.: Conf. Ser.* **571** 1-18

[42] Romanelli G, Hewer B, Krzystyniak M, Gigg M, Tolchenov R, Mukhopadhyay S and Fernandez-Alonso F 2018 Data analysis of neutron Compton scattering experiments using MANTID *Journal of Physics: Conference Series* **1055** 1-18

[43] Andreani C, Degiorgi E, Senesi R, Cilloco F, Colognesi D, Mayers J, Nardone M and Pace E 2001 Single particle dynamics in fluid and solid hydrogen sulphide: an inelastic neutron scattering study *Journal of Chemical Physics* **114** 387–98

[44] Andreani C, Filabozzi A, Pace E and Mayers J 1996 Model-independent analysis of inelastic-neutron-scattering data at high momentum transfer *Phys Rev B* **54** 6255–62

[45] Mayers J and Evans A C 1994 Momentum distributions in fluids determined by neutron compton-scattering *Nuovo Cimento Della Societa Italiana Di Fisica D-Condensed Matter Atomic Molecular and Chemical Physics Fluids Plasmas Biophysics* **16** 737–45

[46] Mayers J 2011 Calculation of background effects on the VESUVIO eV neutron spectrometer *Meas Sci Technol* **22** 1–13

[47] Abdul-Redah T, Krzystyniak M and Chatzidimitriou-Dreismann C A 2005 Neutron Compton scattering from water studied with the double-difference technique *Phys Rev B* **72** 1-3

[48] Andreani C, Ceriotti M, Fernandez-Alonso F, Gorini G, Krzystyniak M, Parmentier A, Parker S, Seel A, Senesi R and Walewski L 2014 Discussion: measurement and instrumentation *J. Phys.: Conf. Ser.* **571** 1-2

[49] Barone V and Cossi M 1998 Quantum calculation of molecular energies and energy gradients in solution by a conductor solvent model *Journal of Physical Chemistry A* **102** 1995–2001

[50] Klamt A and Schüürmann G 1993 COSMO: a new approach to dielectric screening in solvents with explicit expressions for the screening energy and its gradient *Journal of the Chemical Society, Perkin Transactions* **2** 799–805

[51] Ben-Amotz D 2008 Virial theorem and energy partitioning in systems with mixed power-law potentials *Mol Phys* **106** 547–55

[52] McKenzie R H, Bekker C, Athokpam B and Ramesh S G 2014 Effect of quantum nuclear motion on hydrogen bonding *The Journal of Chemical Physics* **140** 1-13

[53] Grech E, Malarski Z and Sobczyk L 1986 Isotopic effects in Nh … N hydrogen-bonds *Chem. Phys. Lett.* **128** 259–63

[54] Novak A 1974 Hydrogen bonding in solids correlation of spectroscopic and crystallographic data *Large Molecules* (Berlin, Heidelberg: Springer Berlin Heidelberg) pp 177–216

[55] Sokolov N D, Vener M V and Savel'ev V A 1990 Tentative study of strong hydrogen bond dynamics: II. Vibrational frequency considerations *Journal of Molecular Structure* **222** 365–86

[56] Huggins M L 1935 Molecular constants and potential energy curves for diatomic molecules *The Journal of Chemical Physics* **3** 473–9

[57] Gidopoulos N I 2005 Breakdown of the born–oppenheimer description explains neutron compton-scattering anomaly *Phys Rev B* **71** 1-5

[58] Krzystyniak M and Fernandez-Alonso F 2011 *Ab initio* nuclear momentum distributions in lithium hydride: Assessing nonadiabatic effects *Phys Rev B* **83** 1-10

[59] Krzystyniak M, Richards S E, Seel A G and Fernandez-Alonso F 2013 Mass-selective neutron spectroscopy of lithium hydride and deuteride: Experimental assessment of the harmonic and impulse approximations *Phys Rev B* **88** 1-16

[60] Webster B C and Buttar D 1992 Zero-point vibrational corrections for the geometry, electric-dipole moment and O-17 nuclear-quadrupole coupling-constant calculated for the muonium isotopomers, muoh and Mu2o, of the water molecule *J Chem Soc Faraday T* **88** 1087–92

[61] Cox S F J 2009 Muonium as a model for interstitial hydrogen in the semiconducting and semimetallic elements *Reports on Progress in Physics* **72** 116501

[62] Mckenna D and Webster B 1984 Non-Adiabatic Calculations Upon the Hydrogen Molecular Ion Isotopically Substituted by Tritium, Deuteron and Muonium *J Chem Soc Farad T* **2** 589–600

[63] Webster B, Hilczer M, Ramos M J and Carmichael I 1985 The inclusion of D-type Gaussian functions in the analytic method for the calculation of electrostatic molecular potentials—interaction of a proton or a positive muon with carbon-monoxide *J Chem Soc Farad T* **2** 1761–9

[64] Claxton T A, Maric D M and Meier P F 1992 Structure of anomalous muonium and the importance of zero-point energy *Chem Phys Lett* **192** 29–33

[65] Lifshitz I M and Kagan Y 1972 Quantum kinetics of phase-transitions at temperatures close to absolute zero *Soviet Physics Jetp-Ussr* **35** 206–20

[66] Storchak V, Cox S F J, Cottrell S P, Brewer J H, Morris G D and Prokofev N V 1996 Muonium localization in solid krypton *Phys Rev B* **53** 662–7

[67] Storchak V G, Eshchenko D G and Brewer J H 2006 Quantum diffusion of muonium atoms in solids: Localization versus band-like propagation *Physica B-Condensed Matter* **374** 347–50